AGU PUBLICATIONS

Geochemistry, Geophysics, Geosystems

RESEARCH ARTICLE
10.1002/2016GC006293

S−to−P heterogeneity ratio in the lower mantle and thermo-chemical implications

Andrea Tesoniero[1], Fabio Cammarano[2], and Lapo Boschi[3,4]

[1]Department of Geosciences and Natural Resource Management, University of Copenhagen, Copenhagen, Denmark, [2]Dipartimento di Scienze Geologiche, Università Roma TRE, Rome, Italy, [3]Sorbonne Universités, UPMC Univ Paris 06, Institut des Sciences de la Terre Paris, Paris, France, [4]CNRS, Institut des Sciences de la Terre Paris, Paris, France

Key Points:
- Robust structural differences between V_P and V_S evidence compositional heterogeneity throughout the mantle and within LLSVPs
- Unconstrained features in seismic models affect $<R_{S/P}>$ profiles and lead to overestimate $R_{S/P}$ in LLSVPs
- Considering uncertainties from mineral physics, it is not possible to reconcile observed seismic structure with a thermo-chemical structure

Correspondence to:
A. Tesoniero,
andrea.tesoniero@ign.ku.dk

Citation:
Tesoniero, A., F. Cammarano, and L. Boschi (2016), S−to−P heterogeneity ratio in the lower mantle and thermo-chemical implications, *Geochem. Geophys. Geosyst.*, *17*, 2522–2538, doi:10.1002/2016GC006293.

Received 1 FEB 2016
Accepted 9 JUN 2016
Accepted article online 13 JUN 2016
Published online 10 JUL 2016

Abstract We evaluate the thermo-chemical state of the lower mantle by analysing the differences in the pattern of heterogeneity between shear and compressional velocity variations and the *S−to−P* heterogeneity ratio ($R_{S/P}=\delta\ln V_S/\delta\ln V_P$) as mapped in our model *SPani* and in alternative joint models. Robust structural differences between V_P and V_S evidence the presence of compositional heterogeneity within the two Large Low Shear Velocity Provinces (LLSVPs). We find also an increasing decorrelation with depth that can be associated with compositional layering of the LLSVPs. In addition, our model shows heterogeneity in the transition zone and mid mantle by complex morphology of subducting slabs and further differences between V_P and V_S that point to an unexpected heterogeneous lower mantle. Precise estimates of compositional heterogeneities are not yet affordable because of the difficulty to provide quantitative measure of $R_{S/P}$, making it difficult to use this ratio to evaluate chemical heterogeneity. For instance, $R_{S/P}$ global median value ($<R_{S/P}>$) drops from ∼2.8 to ∼1.9, at 2500 km depth when the V_P component of *SPani* is replaced by a V_P model resulting from a differently regularized inversion and obtaining an equally good data fit. An increase of 20% of the *SPani* V_P anomalies also drastically reduces $<R_{S/P}>$ without significantly degrading the data fit. Noise in model parameters also leads to overestimate $R_{S/P}$ in the two LLSVPs as we show with synthetic tests. Additional mineral physics uncertainties for compositional effects on $R_{S/P}$ and for the conversion of $\delta\ln V_S$ and $\delta\ln V_P$ into density further complicates a precise chemical interpretation.

1. Introduction

Seismic models are essential to assess the physical properties of the deep structure of the Earth. Owing to the different sensitivity of V_P and V_S to temperature (T) and composition (C), including phase transformations, a comparison of V_P and V_S models provides key information on the physical state of the Earth's interior. In particular, the heterogeneity ratio $R_{S/P}=\delta\ln V_S/\delta\ln V_P$ has been proposed to be an important diagnostic parameter to determine the compositional state of the Earth's mantle [e.g., *Robertson and Woodhouse*, 1996; *Masters et al.*, 2000; *Karato and Karki*, 2001; *Deschamps and Trampert*, 2003]. Observations suggest that $R_{S/P}$ is high in the lowermost mantle, with average values ($<R_{S/P}>$) > 2.5 and especially high values in the region dominated by the two large low shear velocity provinces (LLSVPs) [e.g., *Robertson and Woodhouse*, 1996; *Masters et al.*, 2000; *Della Mora et al.*, 2011].

The thermo-chemical nature of the Earth's lower mantle is still debated. The presence of large $R_{S/P}$ in the two LLSVPs and their sharp edges, the increase of the relative ratio between *S* and *P* velocity variation below 1000 km depth and the anti-correlation between bulk sound velocity variations ($\delta\ln V_\phi$) and shear velocity variations ($\delta\ln V_S$) have been interpreted by several authors as evidence of compositional heterogeneity [e.g., *Trampert et al.*, 2004; *Garnero and McNamara*, 2008; *Della Mora et al.*, 2011]. More recently, other research groups, based on the conversion of global mantle circulation models (MCMs) into elastic parameters [e.g., *Schuberth et al.*, 2009; *Davies et al.*, 2012, 2015], have argued that, although chemical heterogeneities might be present, they are not required to explain the lower mantle seismic observations.

If a map of V_S is to be compared to a map of V_P, they should in principle have the same parameterization and resolution. This is problematic since V_S- and V_P- sensitive data illuminate the Earth's interior in different ways. In spite of this limitation, "joint" inversions where V_P and V_S heterogeneities are unknowns of the same inverse problem are very helpful to study the lower mantle [e.g., *Su and Dziewonski*, 1997; *Hernlund*

and Houser, 2008; *Koelemeijer et al*., 2016]. In *Tesoniero et al*. [2015], we followed this approach, assembling a diverse data set that includes body- and surface-wave (fundamental modes and overtones) observations. We analyze our model *SPani* [*Tesoniero et al*., 2015] to assess the structural and physical properties of the lower mantle region. We identify robust differences between V_P and V_S components of our model and discuss related implications on the structure of thermal and/or chemical heterogeneity of the lower mantle. We anticipate that observed variations throughout the lower mantle and within the LLSVPs suggest that chemical and/or phase related heterogeneity could be more dispersed than what previously thought. In order to infer the chemical nature of those differences, we then focus on the determination of $R_{S/P}$. We show how subtle choices and model parameterization can significantly affect the $S-to-P$ heterogeneity ratio. We compare variations from our inferred spherical-average values ($<R_{S/P}>$), with previously inferred values [e.g., *Robertson and Woodhouse*, 1996; *Antolik et al*., 2003; *Della Mora et al*., 2011] and with values obtained by inverting our V_P or V_S structure for temperature, assuming different compositional models.

2. Data and Tomographic Model

In a previous study [*Tesoniero et al*., 2015, hereinafter paper 1] we jointly inverted Rayleigh and Love surface waves up to the sixth overtone in combination with major *P* and *S* body-wave phases. The inversion scheme also included a regularization constraint in the form of a depth dependent heterogeneity ratio $R_{S/P}$, based on mineral physics estimates. In paper 1, we presented the seismic features of our new model *SPani* and we interpreted the main upper-mantle anomalies in terms of chemical heterogeneities. In this study, we focus our analysis to the lower mantle.

The data coverage is granted by ~1 million of teleseismic direct *P*- and ~250000 *S*- phases (see table 2 in paper 1 for more details). Main *S*- body wave core phases (e.g., *ScS*, *SKS*) are also included, along with multiple bouncing *P*- phases (e.g., *PP*, *PPP*), while the seismic $P-$ body wave data set does not encompass core grazing (e.g., *PcP*) or core traversing (e.g., *PKP*) phases and therefore resolution in the proximity of the core mantle boundary (CMB) drops. We thus mostly focus our analysis and interpretation to the best resolved lower mantle region, i.e. down to ~2600 km depth.

The spatial coverage of data used ensures, within this depth range, a good constraint on both V_P and V_S long-wavelength structure. Different ray-path trajectories of the $P-$ and $S-$ phases and different frequency-dependence of the phases themselves [e.g., *Robertson and Woodhouse*, 1996; *Saltzer et al*., 2001] might slightly affect the modeled structure. In addition, any tomographic inversion requires a series of regularization choices that affect the amplitude of the seismic anomalies and the degree of tomography resolution. In paper 1 we have thoroughly investigated the effects of regularization and weighting on the output model with a systematic analysis [cf. *Tesoniero et al*., 2015, sections 2.6, 2.7, 3.1]. We will here further analyze the role of those effects on the heterogeneity ratio.

3. Seismic Observations

3.1. Lower Mantle Structural Aspects of *SPani*

In *SPani*, the similarity between V_P and V_S structure throughout the lower mantle is remarkable. For example, the degree of similarity measured by the Pearson's correlation coefficient between V_P and V_S ranges from 0.74 to 0.84 between 2000 km and 2500 km depth, and the correlation further increases for longer spatial-wavelength structures. The remaining decorrelation between $\delta \ln V_S$ and $\delta \ln V_P$ holds, however, important information on possible compositional and/or phase variations.

In agreement with other published models, the lower mantle structure of our joint inverted seismic model is dominated by the two LLSVPs beneath Africa and the Pacific ocean (Figure 1). The Pacific anomaly appears to be more scattered in both V_P and V_S compared to the African one. In contrast, the African anomaly shows stronger anomalies and a more continuous shape. Note that this can be partly due to the weaker resolution of the seismic data beneath the South-Eastern Pacific margin as later discussed by using a model resolution analysis. A smoother model could be a possible solution of the inverse problem and would reduce some of the differences between the two macro-regions. In any case, there are robust differences between V_P and V_S that have implications on the thermo-chemical nature of the lower mantle.

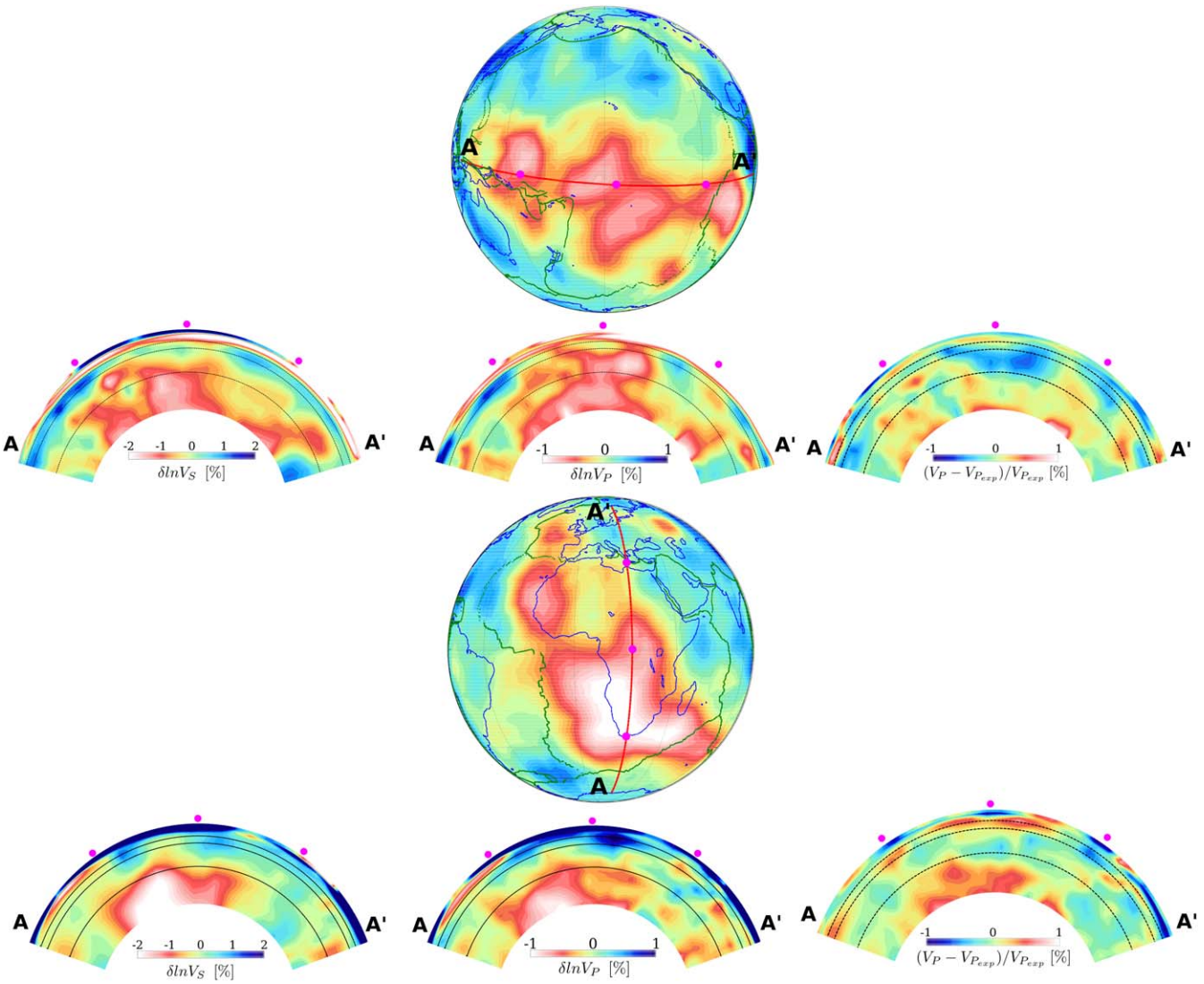

Figure 1. Cross sections through the (top) Pacific and (bottom) African LLSVPs. Three dashed lines at 410 km, 660 km and 1500 km are shown for reference. Maps with profile locations are shear velocity variations at 2500 km depth plotted between $\pm$2% as in the cross sections to the left. The V_P velocity variation is shown in the middle plots cross sections, while the differences between $\delta \ln V_S$ and $\delta \ln V_P$ computed from $\delta \ln V_S$ is shown in the cross sections to the right.

There might be different approaches to quantify the relative variations between V_P and V_S maps. For example, *Hernlund and Houser* [2008] have used a procedure in which they scaled V_P and V_S so that both amplitudes are normalized to a reference V_S standard deviation. Structural differences are then evaluated by considering the misfit $\delta \ln V_S - \delta \ln V_P$ of the normalized values. Here we adopt a similar approach, already used in paper 1, in which we visualize these variations as the difference in percentage between the V_P component of our model and the expected V_P, i.e. a V_P model scaled from our V_S model (see Figure 1 right). As scaling factor, we use the slope of the best linear fit between $\delta \ln V_P$ and $\delta \ln V_S$ distribution at each depth.

The LLSVPs are clearly identified if we look at the V_S part of our model (see Figure 1, left), but the decorrelation between V_P and V_S evidences the presence of robust structural variations within the LLSVPs (Figure 1, right). This observation suggests the presence of compositional heterogeneity within the LLSVPs. Moreover, V_P and V_S in LLSVPs are best correlated in their top part (Figure 1, right), while decorrelation increases toward the bottom of the mantle. This observation is in agreement with the presence of a compositional layering within the LLSVPs [*Ballmer et al.*, 2015], although effects of phase transitions and limited resolution of our model toward the bottom of the mantle complicate a quantitative interpretation. There are other intriguing differences between V_P and V_S structure shown in the cross sections in Figure 1. Note, for

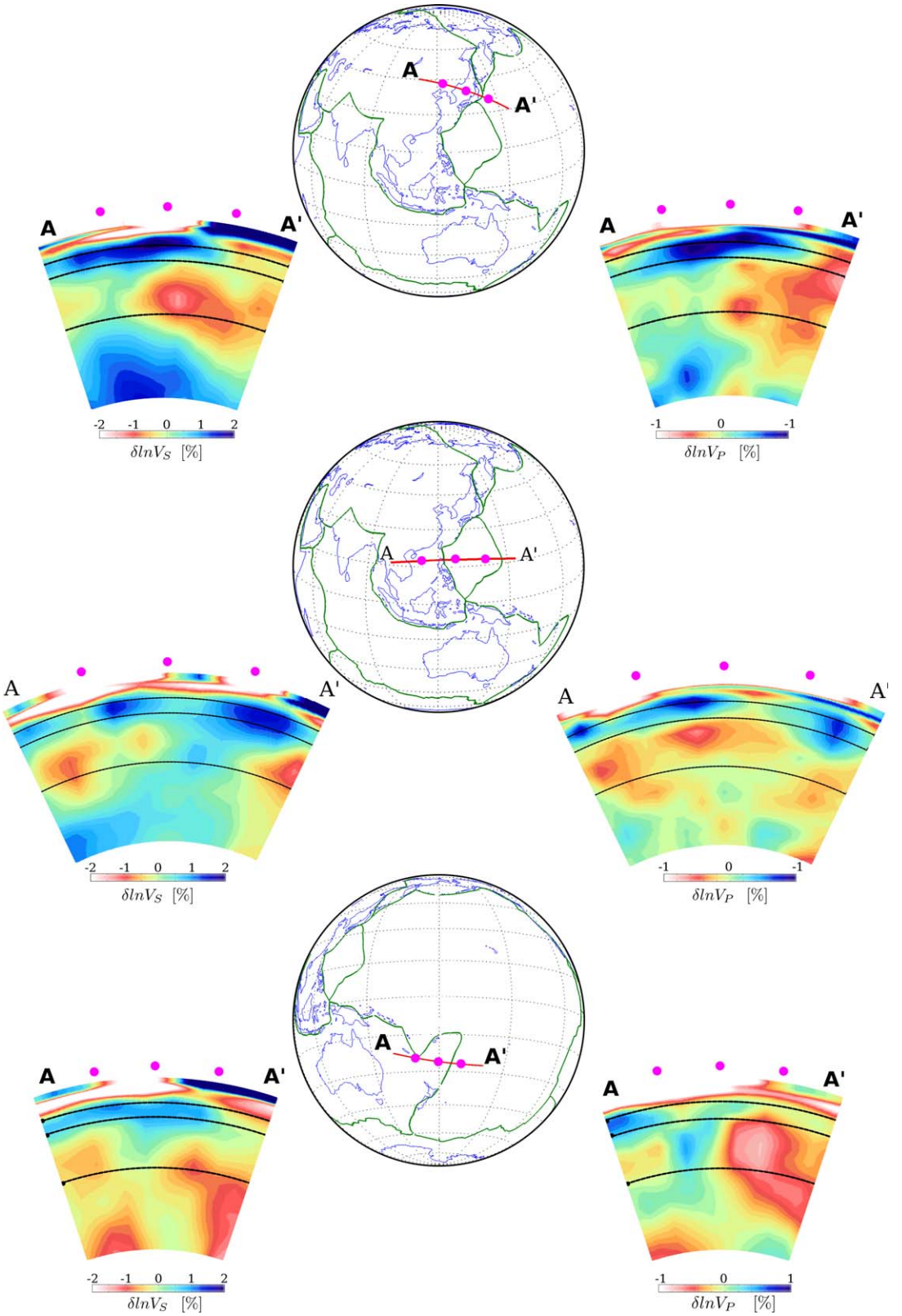

Figure 2. Cross sections from the surface to the CMB across three major convergent margins of the Western Pacific subduction system. From top to bottom we have the northern Honshu arc, the Marianna subducting system and the Tonga Trench. Dashed black lines identify three reference depths of 410 km, 660 km, and 1500 km. The map of V_S is shown to the left side while the V_P is to the right. The slab geometry is consistent between the V_P and V_S model, while a larger degree of decorrelation between V_P and V_S is present below 660 km.

example, the strong V_P anomaly between 700 km and 1500 km depth beneath mid-Pacific that does not correspond to a strong V_S anomaly (Figure 1, top).

In general, we observe differences between $\delta \ln V_P$ and $\delta \ln V_S$ throughout the whole lower mantle and transition zone which suggest a more heterogeneous mantle than previously thought. In Figure 2, we show three cross sections corresponding to subduction regions along the boundary of convergent margins. The slab morphology imaged in our joint tomographic model is overall consistent with that of recent, high-resolution, V_P images [e.g., *Obayashi et al.*, 2013]. In particular, our model shows the same complexity, with slabs that bend and stagnate around 660 km or in the midmantle (∼1000 km). The cross section cutting across the northern Honshu arc in Figure 2 (top) shows, for example, a SE-NW gently dipping slab that sits between 410 km and 660 km depths in both the shear (left) and compressional (right) velocity model comparable to that depicted in *Fukao and Obayashi* [2013, Figure 3]. Interestingly, in spite of limited resolution of our model, we also observe strong V_S anomalies and relatively milder V_P anomalies in the upper mantle above the slabs, which are in agreement with the diffuse presence of fluids and melts (Figure 2, top). Likewise, the morphology of the E-W steeply dipping Marianna slab in Figure 2 (middle) is in agreement with Figure 4 of *Fukao and Obayashi* [2013].

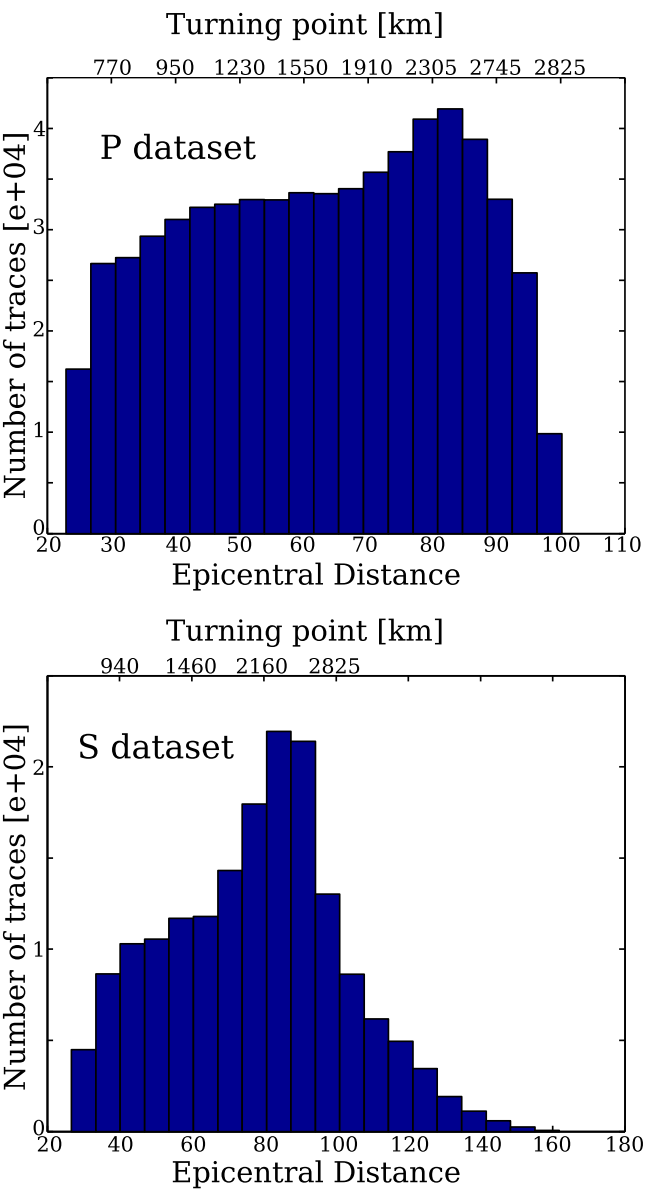

Figure 3. Distribution of (top) direct P and (bottom) direct S data by their epicentral distance.

As previously shown for the cross sections cutting through the African and the Pacific LLSVPs, also the cross sections of Figure 2 are generally characterized by some degree of decorrelation between V_P and V_S. The interpretation of seismic tomography to constrain slab morphology in the mantle is a difficult task. Using either V_P or V_S models can lead, in some cases, to a different shape of fast seismic anomalies associated with slabs. This problem is particularly clear in the Tonga Trench (Figure 2, bottom). Here, the V_S model is characterized by an extensive fast anomaly sitting in the transition zone above 660 km. In the V_P model, instead, a less pronounced positive anomaly seems to image a slab which penetrates deeper in the mantle and stagnates below 1000 km depth.

In general, a precise interpretation of observed discrepancies between V_P and V_S is complicated. A quantitative interpretation of our model requires (a) the precise determination of $R_{S/P}$, and (b) the use of mineral physics relationship to link $\delta \ln V_P$ and $\delta \ln V_S$ to T and C. We first assess, based on synthetic tests, to what extent the differences in the pattern of heterogeneity between the V_P and V_S part of our model (which would imply differences in chemistry) are required by data. We focus on quantitative aspects of our

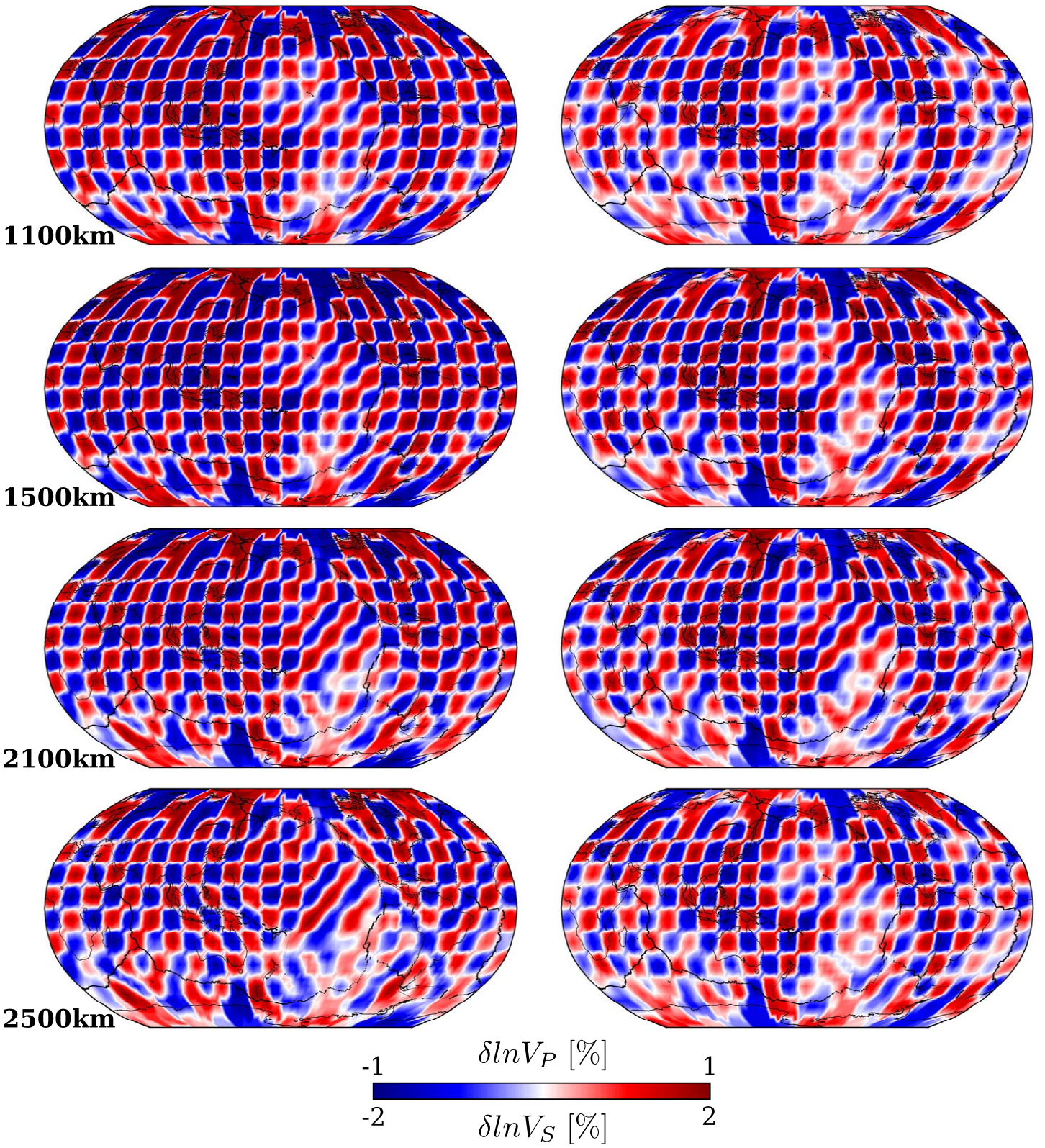

Figure 4. Output of a standard checkerboard resolution test at four lower mantle depths. The amplitude is ±1% for the V_P model and ±2% for the V_S model. The compressional velocity model is on the left side and the shear velocity model on the right. The recovery power of our data set is fairly good both for the compressional and shear velocity model, however the V_P model is better resolved at those depths. The southeastern margin of the Pacific Ocean is rather poorly recovered.

model (and seismic tomographic models more in general) to infer the robustness of the $S-to-P$ heterogeneity ratio. Finally, we make use of current knowledge of material properties to relate observed features to thermo-chemical anomalies.

3.2. Resolution in the Lower Mantle

In paper 1, the global" structural "recovery power of our *P* and *S* data sets has been systematically assessed through several resolution tests, either employing standard checkerboard tests or using tomographic filtering hypothesis techniques [e.g., *Ritsema et al*., 2007, 2009]. These tests were specifically designed to check whether the upper mantle structural features of our tomographic model were robust. In the lower mantle, the resolution of our seismic model depends upon the coverage of our body-wave database. Direct *P* body-wave phases have their turning point in the deep portion of the lower mantle between 2000 and 2800 km depending on the epicentral distance. The double (*PP*) and triple (*PPP*) bouncing *P*-phases provide additional resolution in the upper part of the lower mantle, i.e. below the transition zone and down to 2000 km [e.g., *Koelemeijer et al*., 2016]. We show in Figure 3 the histograms with the distribution of number of traces grouped according to their epicentral distance (and related turning point) for direct *P* and *S* data. We provide here an additional sensitivity test to supplement those shown in paper 1. We use an input model which encompasses a checkerboard pattern of positive and negative velocity anomalies only in the lower mantle region between 1000 km and the CMB. The result shows that the resolution is fairly good throughout the whole lower mantle (Figure 4). Only the regions to the north of the Pacific-Antarctic Rise and to the west of the East Pacific Rise are poorly resolved by our seismic data set.

3.3. The Problem of Estimating $S-to-P$ Heterogeneity Ratio

Seismic tomographic models are a representation of the 3D heterogeneous structure of the Earth's subsurface. Since V_P and V_S heterogeneities differ in both amplitude and wavelength, it is difficult to identify a single value which is representative of a reference V_P and V_S velocity variation at a certain depth. This uncertainty will thus propagate also in $R_{S/P}$ and care must be adopted in defining such a delicate diagnostic parameter.

Different strategies have been adopted to define a representative (1D) depth-dependent profile for $R_{S/P}$. Conventional choices are (i) the mean value [e.g., *Della Mora et al*., 2011], (ii) the median value [e.g., *Masters et al*., 2000; *Davies et al*., 2012], (iii) the ratio of the spherical-average value of the *S* and *P* velocity perturbations [e.g., *Robertson and Woodhouse*, 1996], (iv) the slope of the best linear fit between the V_P and V_S velocity perturbations [e.g., *Saltzer et al*., 2001], (v) the ratio of the *RMS* amplitude between the shear and compressional velocity anomalies [e.g., *Antolik et al*., 2003].

We first remove the 3D average of our model for both V_P and V_S components, and we then compute the $R_{S/P}$ heterogeneity ratio in each point of our model. We consider lateral variations in $R_{S/P}$ at all depths defined by our model's parameterization and we compute their spatial and statistical distribution. We define the average 1D depth profiles $<R_{S/P}>$ by using the median values [e.g., *Robertson and Woodhouse*, 1996; *Masters et al*., 2000; *Davies et al*., 2012]. We discard from our calculations all the values for which $|\delta \ln V_S| < 0.2\%$ and $|\delta \ln V_P| < 0.1\%$, similar to *Della Mora et al*. [2011]. There certainly is an error on both $\delta \ln V_S$ and $\delta \ln V_P$, due to data error and numerical inaccuracy of inversion algorithm. In areas where $\delta \ln V_P$ is close to zero and becomes smaller than the error, the ratio $R_{S/P}=\delta \ln V_S / \delta \ln V_P$ will tend to explode. In areas where the values of both $\delta \ln V_S$ and $\delta \ln V_P$ are smaller than the error, $R_{S/P}$ will have completely meaningless, possibly very large, values. Note that those areas do not pose problems when one just looks at a tomography model: $\delta \ln V_S$ and/or $\delta \ln V_P$ are close to zero and that is correct, within error, but their ratio is not constrained at all (for a short discussion on this issue, see *Della Mora et al*. [2011]). We also discard all the data points for which $\delta \ln V_S$ and $\delta \ln V_P$ have opposite sign variations, resulting in a negative $R_{S/P}$. Note that the $<R_{S/P}>$ is significantly lower if all anomalies are considered. For example, $<R_{S/P}>$ in *SPani* drops from $\sim$2.5 to $\sim$2, at 2500 km depth, if also small and opposite sign anomalies are considered.

3.4. Implications of Tomographic Regularization (Smoothing)

The global tomography inverse problem is notoriously ill-conditioned. Consequently, seismic tomography requires one or more regularization constraints to stabilize the inversion and achieve a meaningful solution. In this section, we investigate the effects that different regularization constraints have on the retrieved spherical-average $<R_{S/P}>$ in the lower mantle. We performed two inversions in which we changed the

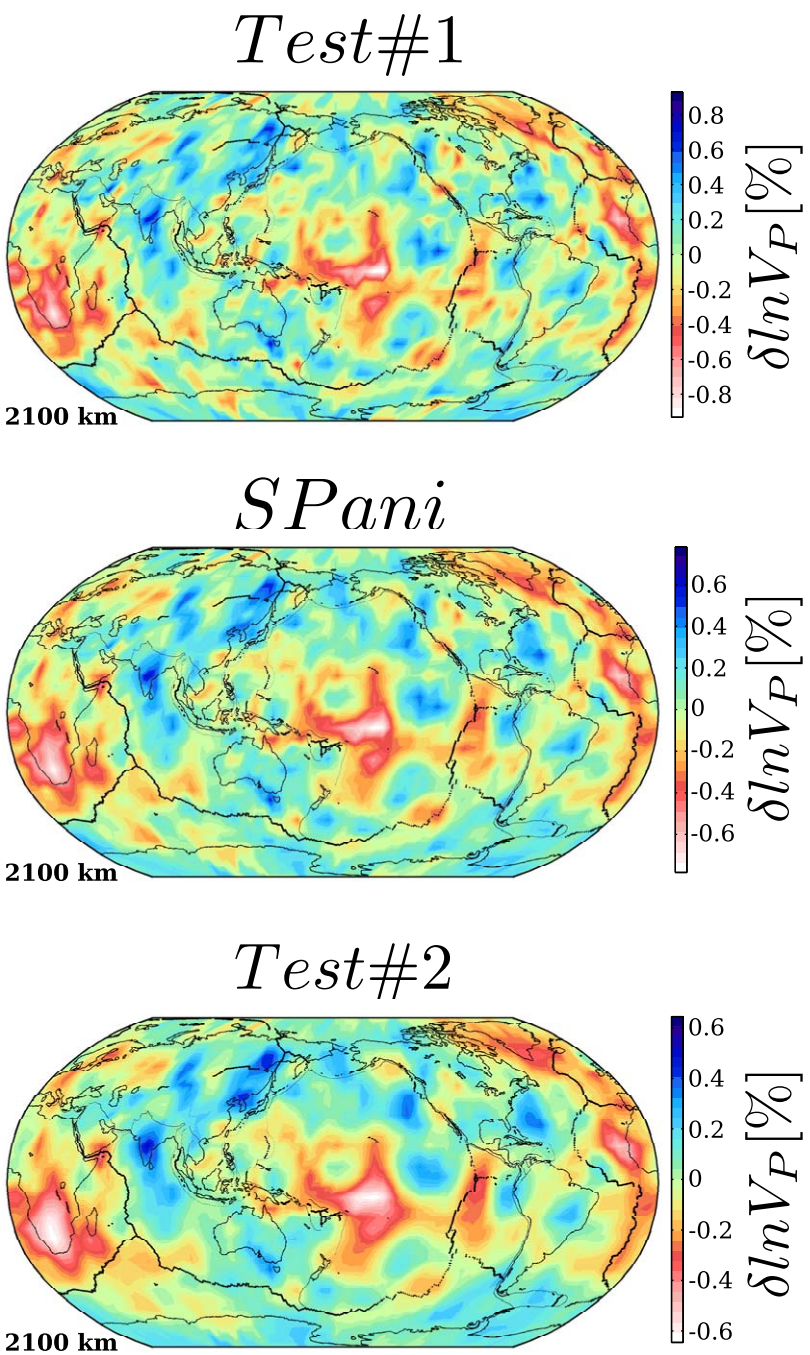

Figure 5. Compressional velocity variations at 2100 km depth for three models with different roughness damping. The roughness damping increases from top to the bottom. Note how, as the model becomes smoother, the amplitudes of the anomalies become smaller, thus strongly influencing the retrieved $R_{S/P}$.

roughness damping parameter (*rdp*) of the V_P component of our model with respect to the V_S component between 1000 and ~2700 km depth. In the first test, the *rdp* for V_P is chosen to be half of that of the V_S model, while in the second test we double the *rdp* of V_P with respect to V_S. This way, we allow for larger lateral velocity jumps than *SPani* in the first case (*Test#1*), and, in the second case, we constrain the seismic anomalies to be more similar between neighbooring blocks, thus obtaining a smoother model than *SPani* (*Test#2*). As expected, the amplitudes of V_P anomalies are larger than *SPani* in *Test#1* and smaller in *Test#2*.

The large-scale structural features of the two test models are very similar to our favorite model *SPani* (see Figure 5). All models show a good overall data fit (around 80%) but large differences arise in their spherical-average $R_{S/P}$ profiles. Specifically, the smoother model is characterized by significantly higher $<R_{S/P}>$ compared to the less smooth one (Figure 6). Interestingly, at a depth of 2500 km, the median value of $R_{S/P}$ has a value around 2.7 for the smooth model, while the value drops to ~2 in the case of *Test#1*. A common feature between all the models is the increase with depth of the heterogeneity ratio, although with a different gradient, throughout the lower mantle (Figure 6).

Finally, note that the all the seismic models span a large range of $R_{S/P}$ at each depth, as shown by the shadowed area in Figure 6, which marks the 25^{th} and 75^{th} percentiles of *SPani* values.

3.5. $R_{S/P}$ Lateral Variations

In the last two sections, we shortly mentioned the presence of relevant decorrelations between V_P and V_S anomalies (Figure 1) and a wide statistical distribution of $<R_{S/P}>$ (Figure 6). In this section, we further examine how lateral variations are constrained by seismic data since their determination has important implications for compositional structure. In agreement with previous studies, *SPani* shows high heterogeneity ratios in well imaged LLSVPs in the lower mantle. This observation has been used to interpret LLSVPs as chemically differentiated regions from the surrounding mantle [e.g., *Su and Dziewonski*, 1997; *Masters et al*., 2000; *Wen et al*., 2001; *McNamara and Zhong*, 2005]. A statistical analysis of the lower mantle shows that $R_{S/P}$ grows with increasing absolute values of velocity anomalies, be they positive or negative (Figure 7, top). The same pattern is also reproduced in other joint V_P and V_S tomographic models *hmsl06* [*Houser et al*., 2008] and *GyPSum* [*Simmons et al*., 2010] (Figure 7, bottom). The *GyPSum* model also presents peculiar features, such as fingerlike trends and cutoff values (Figure 7, bottom-right), that are likely due to the adoption of more stringent mineral physics constraints in the inverse process (we note that geodynamic observations have been also inverted in this model). The observed trend does not have any physical meaning and it emerges if small random decorrelations between V_P and V_S structure exist.

In order to document this, we present the results of suite of synthetic tests, performed using 100 test models, designed to quantify to what extent the degree of decorrelation between V_P and V_S is a physical characteristic of our joint model or if it is an artifact due to e.g., noise in the model parameters. The tests are performed into two steps:

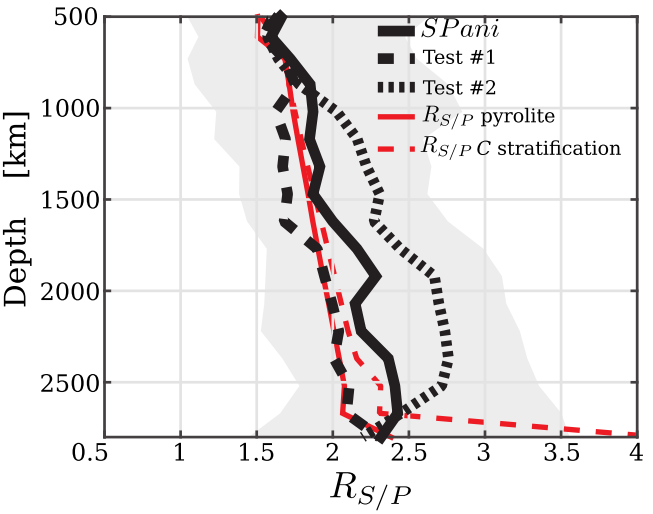

Figure 6. Spherical-average heterogeneity ratio $<R_{S/P}>$ for SPani (solid black line) compared to $<R_{S/P}>$ for two test models (black dashed and dotted lines). Test#1 (dashed black) is a model with enhanced roughness in V_P structure and Test#2 (dotted black) has a smoother (less rough) V_P. The shaded region is delimited between the 25^{th} and 75^{th} percentiles of SPani $<R_{S/P}>$. The red curves show the ratios obtained by converting the V_S component of SPani into V_P (and temperature) assuming pyrolitic composition (solid red line) or a chemically stratified composition (dashed red line) with MORB enrichment with depth (see main text).

1. The V_P component of our model *SPani* between 1000 km and the CMB is initially scaled to V_S so that the correlation between the two seismic structures is equal to 100%
2. Gaussian random noise is added to the perfectly scaled model until the degree of correlation between V_P and V_S matches the one observed in *SPani*
3. A comparison between the the original model and the one contaminated with white noise is carried out by looking at the statistical distribution of the $V_P - V_S$ anomalies, of $R_{S/P} - \delta \ln V_S$ and the histograms of the $R_{S/P}$ distributions.

An example is shown in Figure 8 for one test model and for a depth of 2070 km. For all the 100 tests models, a Gaussian noise with a standard deviation ~16% is sufficient to reproduce the same statistical distribution in the

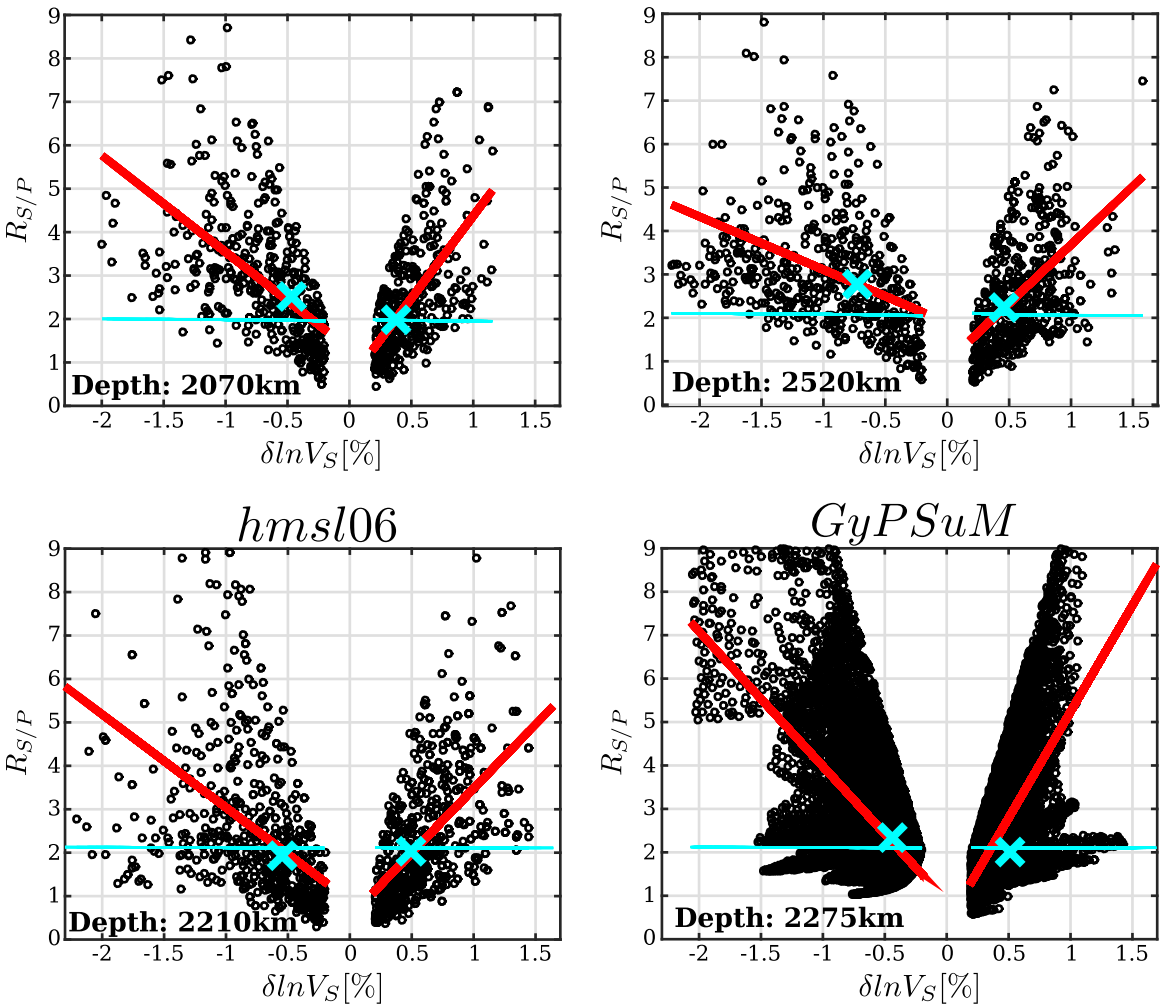

Figure 7. Heterogeneity ratio against V_S variations are shown (top) at two depths for SPani, and at one depth each (bottom) for hmsl06 [*Houser et al.*, 2008] and (bottom right for GyPSuM [*Simmons et al.*, 2010]. Small $R_{S/P}$ anomalies ($|\delta \ln V_S| < 0.2\%$ and $|\delta \ln V_P| < 0.1\%$) and opposite sign anomalies are not considered. Red lines are linear interpolation of positive and negative anomaly branches. Cyan crosses identify the point whose x and y coordinate are, respectively, the median value of the V_S variations and the median heterogeneity ratios. Cyan lines are expected $R_{S/P}$ from purely thermal interpretation of $\delta \ln V_S$ assuming pyrolite. Note that $R_{S/P}$ tends to increase as the anomalies, either positive or negative, increase.

$\delta \ln V_P - \delta \ln V_S$ plane we observe in *SPani* (Figure 8, middle and right). As random noise is added, the distribution of $R_{S/P}$ starts to spread out and reproduces the trend with higher $R_{S/P}$ values for large $\delta \ln V_S$ anomalies (compare middle-top and middle-bottom plots in Figure 8). Since the distribution of $R_{S/P}$ of our synthetic model is very similar to *SPani*, the global median value and the median value only computed in low velocity regions, i.e. regions where $\delta \ln V_S < -1$ (Figure 8, right), are also well reproduced. This suggests that the relatively high $R_{S/P}$ values in LLSVPs can be biased by "noise" in the model parameters. The relation between V_P and V_S heterogeneity, and behaviour of $R_{S/P}$ observed from *SPani* (Figure 8, top) can thus reflect both a "real decorrelation" between $\delta \ln V_S$ and $\delta \ln V_P$, or the effect of relatively small errors in tomography models that propagate into $R_{S/P}$ and affect it significantly. Given the notorious resolution problems of global tomography, the latter interpretation might be very important.

Importantly, the white-noise added has a small effect on data-fit: all 100 synthetic test-models are characterized by similar data-fit. The fit for *P* data is always almost the half of the original model (decreasing from ~41% to ~19%) and indicates that part of the differences between V_P and V_S in our model is robust and indeed required by the data.

Another limitation in tomography images is related to the amplitudes of the anomalies. We tested that an increase of 20% of the V_P anomalies (i.e. $\delta \ln V_P' = \delta \ln V_P + 20\% \cdot \delta \ln V_P$) reduces $<R_{S/P}>$ from 3 to 2.5 without significantly degrading the data-fit. The fit for *P*-wave travel times drops from 40.9% in *SPani* to 40% for the model with the increased V_P anomalies.

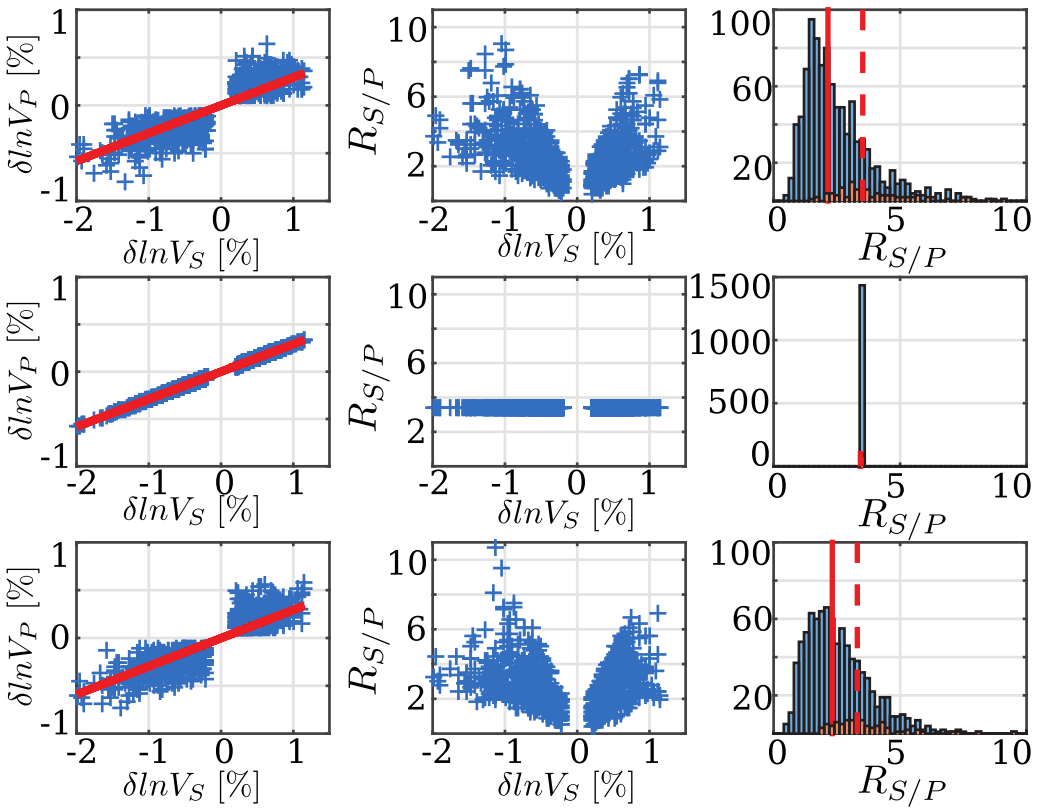

Figure 8. (top) Distribution of (left) $V_S - V_P$ velocity perturbations, (middle) V_S velocity perturbation versus $R_{S/P}$ and (right) histogram with $R_{S/P}$ distribution calculated for model SPani at 2070 km depth. (middle) likewise top plots but replacing the V_P component of SPani with a synthetic V_P perfectly scaled from V_S. (bottom) White noise is added to the perfectly scaled model of the middle plots until the same correlation coefficient of SPani is reached. (right) Red histograms are only computed in areas where $\delta \ln V_S < -1\%$. Solid red lines in right plots are the global median values while dashed lines are the median values only for low-velocity regions.

To furthermore document the important role of regularization in distribution of $R_{S/P}$ values, we show the results of a "tomographic filtering hypotheisis" resolution test [*Ritsema et al*., 2009] performed in paper 1. For this test, we used as input model the geodynamic mantle convection model by *Bello et al*. [2015], which has several Earth-like features (although it does not posses LLSVPs). V_P and V_S are perfectly correlated (Pearson correlation coefficient $CC = 100\%$) in the input model and $R_{S/P}$ value is uniform and equal to 2. We obtain an output model by using our inversion algorithm. Although the correlation coefficient degrades only slightly ($CC \simeq 0.96\%$), the range of $R_{S/P}$ values becomes extremely large, from ~ -1 to ~ 6 (Figure 9).

4. Interpretation and Discussion

4.1. Comparison With Mineral Physics

We convert our V_S structure to temperature and V_P (or V_P to temperature and V_S) assuming different compositional structures. Equilibrium mineralogies and physical properties (V_P, V_S and density) as a function of pressure, temperature and composition have been obtained by thermodynamical modeling, using Perple-X [*Connolly*, 2009]. All the computations are based on the thermodynamical database by *Stixrude and Lithgow-Bertelloni* [2011] based on a 6 oxides system (Na-Ca-Fe-Mg-Al-Si), already used by *Cammarano et al*. [2011], and also include pressure- (P) and temperature- (T) dependent anelasticity effects [*Cammarano et al*., 2003]. For a given composition, absolute temperatures can be thus inferred if absolute seismic velocities are available. We retrieve absolute V_S and V_P values by assuming correct the values of the reference 1D seismic model.

We consider two end-member compositional structures without lateral variations. First, we consider a pyrolitic composition, either as a thermodynamically equilibrated assemblage or as a mechanical mixture (i.e. an assemblage of chemical components that do not chemically mix) of MORB (20%) and Harzburgite (80%).

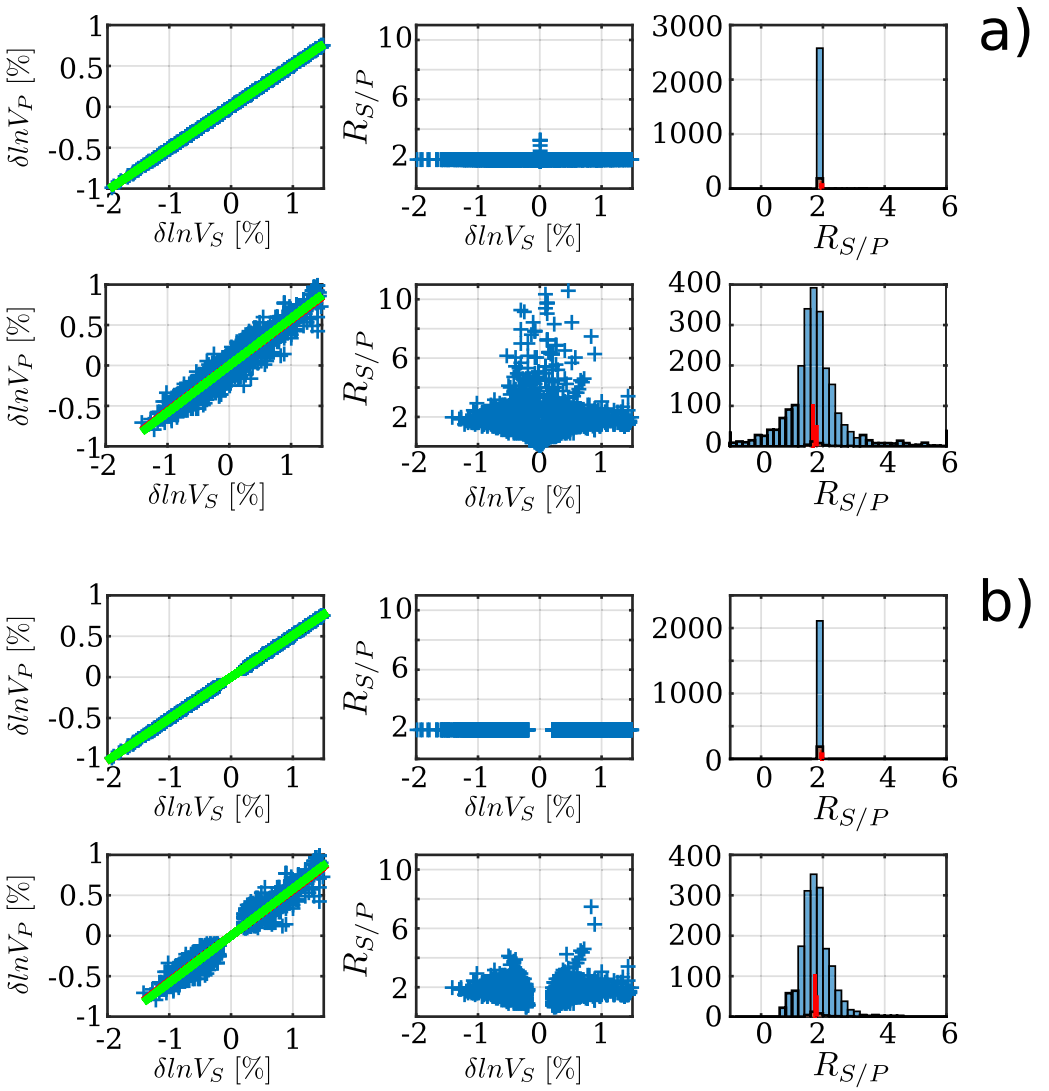

Figure 9. Same analysis presented in Figure 8 for the "tomographic filtering hypothesis test" using the mantle convection model of *Bello et al.* [2015] for two cases: (a) one in which all the points are considered and (b) one in which small and opposite-sign anomalies are omitted. (top) Input model and (bottom) recovered output model. The correlation coefficient between V_S and V_P changes from $CC=100\%$ for the input model, to $CC=96\%$ in the output model.

The two cases do not produce significant variations for what concerns the spherically average $R_{S/P}$ profile, therefore we only show in Figure 6 the result for a mechanical mixture (red lines). Second, we test a compositional structure that captures the chemical stratification obtained in geodynamical mantle convection models [e.g., *Tackley et al.*, 2005; *Nakagawa et al.*, 2010]. Namely, we model a mechanical mixture made of 10% MORB (and 90% Harzburgite) just below 660 km depth which linearly increases in MORB content, reaching 80% MORB (and 20% Harzburgite) at the CMB. In spite of the uncertainties in mineral physics parameters, well described in *Cobden et al.* [2009], the deviation in terms of $<R_{S/P}>$ profiles between two compositional models that entail totally different geodynamic scenarios is very small (Figure 6, red lines). Indeed, seismic models with a slightly different roughness damping parameter are characterized by larger variations in $<R_{S/P}>$ as illustrated in Figure 6 by the black curves.

The increasing trend with depth is generally well reproduced by models with purely thermal variations, such as the two shown in red in Figure 6. Only relatively small deviations around the mean emerge in correspondence of mineralogical phase transitions.

Since the seismically observed large range of lateral variations in $R_{S/P}$ cannot be reproduced by thermal variations alone, we test the effects of lateral compositional variations on spherical-average $R_{S/P}$. We carried

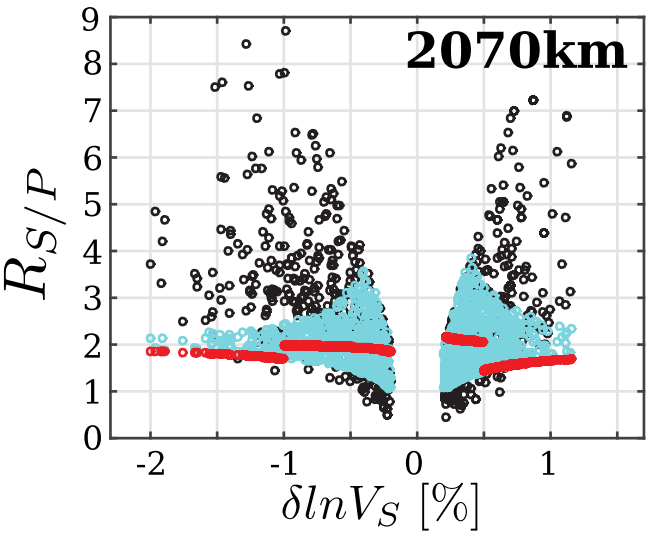

Figure 10. Heterogeneity ratio against VS variations for a layer centered at 2070 km depth. Black circles refer to the values in model SPani. Cyan circles are values obtained by inverting V_S for a randomly perturbed compositions between harzburgite and 40% MORB, red circles are values obtained by assigning MORB composition in regions where $\delta \ln V_S < -1$ and harzburgite composition where $\delta \ln V_S > 0.5$.

out two tests: (i) we introduce random small-scale differences between an extremely depleted (100% harzburgite) and a depleted (40% MORB, 60% harzburgite) composition; (ii) we associate the large negative shear-velocity provinces in the lower mantle (we arbitrarily choose $\delta \ln V_S < -1\%$) with an enriched composition (40% MORB) and fast anomalies ($\delta \ln V_S > 0.5$) with Harzburgite. The spherical-average profiles do not significantly change from the compositional models without lateral variations shown in Figure 6, but we now span a large, even though smaller of what seismically observed, range of variations (see Figure 10). Assuming MORB enrichment in LLSVPs results in slightly lower $R_{S/P}$ and not higher (Figure 10) which is in agreement with the results derived from synthetic global models [e.g., *Davies et al*., 2012]. This result is due to the fact that, according to our mineral physics database, MORB composition is faster in V_S than in V_P compared to a reference pyrolitic mantle. For example, at a temperature of 2000 K and at 2070 km depth, MORB V_S is ∼1.5% faster than pyrolite and V_P is only ∼0.2% faster. This result is in conflict with the result of *Cobden et al*. [2009], which obtained for a similar Si-rich and Mg-poor composition a stronger effect on V_P than on V_S, and most likely depends on the role that sodium has in stabilizing the Ca-Ferrite (CF) phase (neglected in *Cobden et al*. [2009]).

It is not possible to obtain the observed trend toward high $R_{S/P}$ both in relatively slow and fast regions (Figure 7), confirming the lack of a physical meaning of this feature. As we showed previously, this trend can easily be obtained adding small decorrelation between V_P and V_S structure. This is also the case for the relatively high median values of $R_{S/P}$ in LLSVPs compared to global median (Figure 7) which can be originated by the same mechanism. In conclusion, our attempt of interpreting V_P and V_S structure is complicated by the limitation in tomography imaging and by uncertainties in the mineral physics.

4.2. Are Large-Scale Chemical Anomalies Required in Correspondence of LLSVPs?

In spite of its limitations, seismic tomography provides the best resolved images of the deep Earth's interior. In *SPani*, we considered a very large seismic database which includes $P-$ and $S-$ body waves, surface waves and overtones. We show here that small perturbations in tomography regularization parameters can have significant consequences for the determination of $R_{S/P}$ (and also for the indirect determination of $R_{\phi/S}$, the relative ratio between bulk-sound and shear-velocity). In particular, seismic data do not tightly constrain high values of the $S-to-P$ heterogeneity ratio in LLSVPs. This result, however, does not preclude that these large regions are chemically different than surrounding mantle. In addition, as shown in Figure 1, most of the structural differences between $\delta \ln V_S$ and $\delta \ln V_P$ (but not all and not in a uniform manner) occur within the LLSVPs. As a matter of fact, an extremely chemically enriched composition can have a mild effect on $R_{S/P}$ (e.g., see Figure 10).

Density is an important discriminating factor between thermal and compositional effects [e.g., *Forte and Mitrovica*, 2001; *Deschamps and Trampert*, 2003], but lateral variations are only poorly resolved by gravity (and geoid) observations and by seismic data (i.e., low-frequency normal modes [e.g., *Ishii and Tromp*, 2004]). Density models obtained from combined interpretation of geodynamic and seismic observations [e.g., *Simmons et al*., 2010; *Ishii and Tromp*, 2004] show an anti-correlation between density and V_S toward the bottom of the mantle (where our model lacks resolution) which would require a chemical explanation. However, sensitivity to density variations is weak close to the CMB [*Romanowicz*, 2001]. A combination of

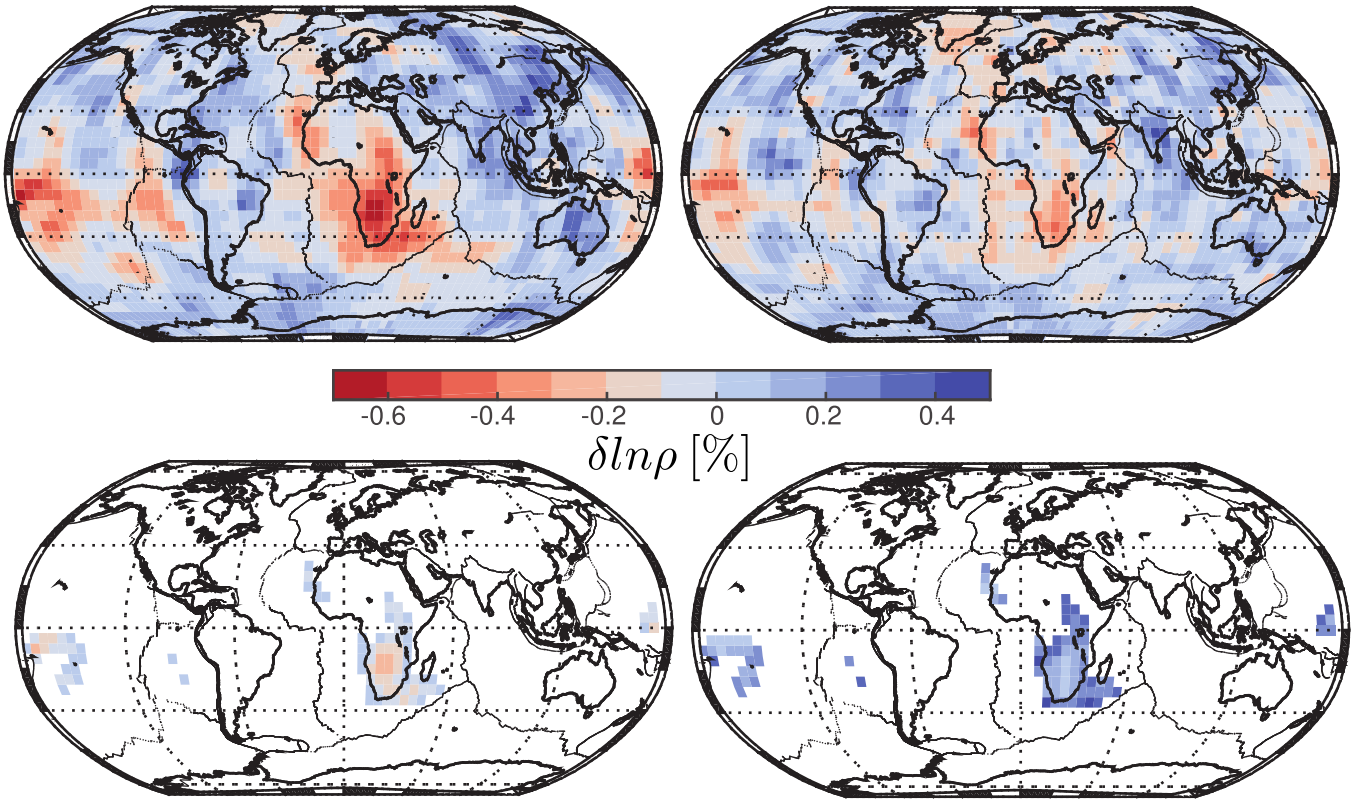

Figure 11. Relative density variations at 2100 km depth inferred from (left) V_S and (right) V_P of SPani. (top) Purely thermal density structure assuming pyrolite composition. (bottom) Effects of composition on density contrast: MORB chemical composition is assumed in regions with $\delta \ln V_S < -1\%$, which are associated with LLSVPs.

body waves and core-sensitive normal modes into the same tomographic inversion can increase the constraint on the density and seismic structure in the CMB region [*Houser*, 2007]. In our joint V_P and V_S inversion, we did not invert for density. We can, however, predict density structure by interpreting the seismic structure using mineral physics relationships. Large uncertainties exist. The most evident problem is the incompatibility between thermal interpretation of V_P and V_S structure using the same compositional structure [e.g., *Cammarano et al*., 2005; *Davies et al*., 2015] and thus on lateral density contrasts. A purely thermal interpretation of V_S, assuming pyrolite, gives LLSVPs that are ∼20% hotter than mean temperature at 2100 km depth, and around 0.7% less dense than average density at the same depth (Figure 11). Much smaller temperature and density contrasts, respectively ∼10% and ∼0.35% at 2100 km depth, are obtained by converting the V_P structure with the same composition and mineral physics database.

According to our computation, a MORB composition for LLSVPs (we consider regions with $\delta \ln V_S < -1\%$) would have negligible effects on thermal contrasts, but strongly affects the density structure. We compute slightly hotter LLSVPs, i.e ∼22%, interpreting V_S and around the same previous value, i.e ∼10%, assuming V_P. Since MORB is significantly denser than pyrolite at the same $P-T$ conditions, the density contrast due to thermal effects is largely, but not entirely, balanced by a MORB chemical composition in the case V_S is interpreted (Figure 11, bottom-left), and LLSVPs become even denser than surrounding mantle (around 0.15% at 2100 km) in case of less strong thermal contrasts predicted from V_P.

We are not able to find a compositional model that is consistent with our data. However, in light of the limited sensitivity to density structure of the lower mantle and of large uncertainties from mineral physics, we cannot draw a final conclusion on the presence or absence of large-scale chemical anomalies at the LLSVPs.

4.3. Resolution of $R_{S/P}$

It is conventionally assumed that seismic anomalies with values of $R_{S/P} > 2.5$ require also compositional and/or phase related effects beside temperature to be explained [e.g., *Karato*, 1993; *Karato and Karki*, 2001].

Spherical-average $R_{S/P}$ has been used as an indicator of compositional anomalies in the lower part of the mantle [e.g., *Deschamps and Trampert*, 2003]. Moreover, high values of $R_{S/P}$ in LLSVPs are in agreement with the presence of chemically dense piles of hot material.

We have analyzed our joint V_P-V_S tomographic model to estimate the $S-to-P$ heterogeneity ratio and its spherical-average profile. We found values of $<R_{S/P}>$ in the lower mantle which are lower than what inferred from previous seismic studies and not higher than 2.5. More importantly, we have shown how the statistical distribution of $R_{S/P}$ is extremely sensitive to the model parameterization and regularization. Therefore, any average estimate (e.g., mean, median) of $R_{S/P}$, at a given depth, is not well constrained by seismic data. Information derived from synthetic tests show that the width of the histograms, the high value of $R_{S/P}$ within the LLSVPs, and the increasing trend of $R_{S/P}$ for both positive and negative velocity anomalies, can be replicated in models perturbed with random noise. This result is in disagreement with what proposed by *Deschamps and Trampert* [2003] for which the dispersion of the histograms contains qualitative information of compositional anomalies.

Older low resolution models, for example the model of *Robertson and Woodhouse* [1996], are characterized by very high values (e.g., 2.7 at 2000 km depth). Similar values can be also obtained by smoothing *SPani* in spherical harmonics down to degree 8. A more subtle effect is related to the choice of regularization parameters. We have shown that slight variations in the roughness damping parameters between V_P and V_S can have significant effects on the estimated $<R_{S/P}>$, although the data fit remains substantially unchanged. Specifically, the variation in $<R_{S/P}>$ with models with slightly different roughness exceeds the theoretical variation in $R_{S/P}$ profile between two extremely different (1D) compositional structures (Figure 6).

The slope of the best (orthogonal) linear fit between the V_P and V_S velocity perturbations should be a more robust indicator for $<R_{S/P}>$ since it is not affected by noise in the model parameters. However, as discussed in section 3.5, seismic data do not tightly constrain the amplitudes of the anomalies, and this will affect obtained slopes.

Our results evidence the difficulty to extract a robust physical interpretation on the basis of a specific seismic model and the risk of over-interpreting the model. Some of the model features which are not strictly required by the data can have, if interpreted, important implications for the nature of the mantle.

5. Conclusion

We have extended the analysis of our shear and compressional tomographic velocity model *SPani* [*Tesoniero et al*., 2015] to the lower mantle structure with the aim of interpreting lower mantle seismic anomalies in terms of temperature and composition.

We found robust structural differences between V_P and V_S within the LLSVPs and an increasing decorrelation toward the bottom of the mantle. The two observations suggest a possible compositional layering within the LLSVPs and question the interpretation of LLSVPs as isolated thermo-chemical piles. The morphology of subducting slabs and differences between V_P and V_S show a complex pattern, with some slabs which deflect and stagnate in the transition zone and others at greater depth. In summary, the robust structural features indicate a complex lower mantle and suggest a dispersed chemical heterogeneity throughout the mantle.

In order to better interpret model *SPani*, we assessed how well the structural variations and the $S-to-P$ heterogeneity ratio can be determined from seismic data. Our analysis shows that the definition of the spherical-average value of the $S-to-P$ heterogeneity ratio can lead to different estimates and that the statistical distribution of $R_{S/P}$ is strongly biased by specific choices in model's parameterization and regularization, as already reported in *Hernlund and Houser* [2008]. Small decorrelations between $\delta \ln V_P$ and $\delta \ln V_S$ do not significantly deteriorate our ability to detect the structure, but they do significantly alter the statistical distribution of $R_{S/P}$ and lead to overestimate $R_{S/P}$ in LLSVPs. Lateral variations in $R_{S/P}$ are also affected by the limited sensitivity of seismic data to the amplitude of the anomalies. Owing to large mineral physics uncertainties, low values of $R_{S/P}$ cannot, however, exclude the presence of large-scale chemical heterogeneity.

We found that temperature variations, and associated density contrasts based on given compositional structures, significantly vary if V_P or V_S are interpreted. Albeit biased by the limited sensitivity to seismic

anomalies amplitudes, and by the large uncertainties in high pressure-temperature mineral physics, this result might indicate the possibility for chemical heterogeneity. A systematic search to find the most likely thermo-chemical structure for geophysical data, properly dealing with all uncertainties involved, emerges as an indispensable tool for the future. Our results also call for a better characterization, at high pressures and temperatures, of the seismic velocity of Earth materials.

Acknowledgments
We are thankful to Rhodri Davies and Christine Houser whose contribution helped us to improve the manuscript, and to the several authors for sharing their data. The joint tomographic velocity model is available on the IRIS-EMC webpage at http://ds.iris.edu/ds/products/emc-spani/. The original model bundle can be downloaded at https://github.com/atesoniero/SPani. This work is supported by Danish Research Council, Sapere Aude grant 11-105974.

References

Antolik, M., Y. J. Gu, G. Ekström, and A. M. Dziewonski (2003), J362D28: A new joint model of compressional and shear velocity in the Earth's mantle, *Geophys. J. Int.*, *153*(2), 443–466, doi:10.1046/j.1365-246X.2003.01910.x.

Ballmer, M. D., N. C. Schmerr, T. Nakagawa, and J. Ritsema (2015), Compositional mantle layering revealed by slab stagnation at ~1000-km depth, *Sci. Adv.*, *1*(11), doi:10.1126/sciadv.1500815.

Bello, L., N. Coltice, P. J. Tackley, D. Müller, and J. Cannon (2015), Assessing the role of slab rheology in coupled plate-mantle convection models, *Earth Planet. Sci. Lett.*, 191–201, doi:10.1016/j.epsl.2015.08.010.

Cammarano, F., S. Goes, P. Vacher, and D. Giardini (2003), Inferring upper-mantle temperatures from seismic velocities, *Phys. Earth Planet. Inter.*, *138*(3-4), 197–222, doi:10.1016/S0031-9201(03)00156-0.

Cammarano, F., A. Deuss, S. Goes, and D. Giardini (2005), One-dimensional physical reference models for the upper mantle and transition zone: Combining seismic and mineral physics data, *J. Geophys. Res.*, *110*, B01306, doi:10.1029/2004JB003272.

Cammarano, F., P. Tackley, and L. Boschi (2011), Seismic, petrological and geodynamical constraints on thermal and compositional structure of the upper mantle: Global thermochemical models, *Geophys. J. Int.*, *187*(3), 1301–1318, doi:10.1111/j.1365-246X.2011.05223.x.

Cobden, L., S. Goes, M. Ravenna, E. Styles, F. Cammarano, K. Gallagher, and J. A. D. Connolly (2009), Thermochemical interpretation of 1-D seismic data for the lower mantle: The significance of nonadiabatic thermal gradients and compositional heterogeneity, *J. Geophys. Res.*, *114*, B11309, doi:10.1029/2008JB006262.

Connolly, J. A. D. (2009), The geodynamic equation of state: What and how, *Geochem. Geophys. Geosyst.*, *10*, Q10014, doi:10.1029/2009GC002540.

Davies, D., S. Goes, and H. Lau (2015), Thermally dominated deep mantle LLSVPs: A review, in *The Earth's Heterogeneous Mantle, Springer Geophys.*, edited by A. Khan and F. Deschamps, chap. 14, pp. 441–477, Springer Int. Publ., Cham., doi:10.1007/978-3-319-15627-9_14.

Davies, D. R., S. Goes, J. Davies, B. Schuberth, H.-P. Bunge, and J. Ritsema (2012), Reconciling dynamic and seismic models of Earth's lower mantle: The dominant role of thermal heterogeneity, *Earth Planet. Sci. Lett.*, *353-354*, 253–269, doi:10.1016/j.epsl.2012.08.016.

Della Mora, S., L. Boschi, P. J. Tackley, T. Nakagawa, and D. Giardini (2011), Low seismic resolution cannot explain S/P decorrelation in the lower mantle, *Geophys. Res. Lett.*, *38*, L12303, doi:10.1029/2011GL047559.

Deschamps, F., and J. Trampert (2003), Mantle tomography and its relation to temperature and composition, *Phys. Earth Planet. Inter.*, *140*(4), 277–291, doi:10.1016/j.pepi.2003.09.004.

Forte, A. M., and J. X. Mitrovica (2001), Deep-mantle high-viscosity flow and thermochemical structure inferred from seismic and geodynamic data, *Nature*, *410*, 1049–1056, doi:10.1038/35074000.

Fukao, Y., and M. Obayashi (2013), Subducted slabs stagnant above, penetrating through, and trapped below the 660 km discontinuity, *J. Geophys. Res. Solid Earth*, *118*, 5920–5938, doi:10.1002/2013JB010466.

Garnero, E. J., and A. K. McNamara (2008), Structure and dynamics of earth's lower mantle, *Science*, *320*(5876), 626–628, doi:10.1126/science.1148028.

Hernlund, J. W., and C. Houser (2008), On the statistical distribution of seismic velocities in earth's deep mantle, *Earth Planet. Sci. Lett.*, *265*(34), 423 – 437, doi:10.1016/j.epsl.2007.10.042.

Houser, C. (2007), *Constraints on the Presence or Absence of Post-Perovskite in the Lowermost Mantle from Long-Period Seismology*, pp. 191–216, AGU, Washington, D. C., doi:10.1029/174GM14.

Houser, C., G. Masters, P. Shearer, and G. Laske (2008), Shear and compressional velocity models of the mantle from cluster analysis of long-period waveforms, *Geophys. J. Int.*, *174*(1), 195–212, doi:10.1111/j.1365-246X.2008.03763.x.

Ishii, M., and J. Tromp (2004), Constraining large-scale mantle heterogeneity using mantle and inner-core sensitive normal modes, *Phys. Earth Planet. Inter.*, *146*(1-2), 113–124, doi:10.1016/j.pepi.2003.06.012.

Karato, S. (1993), Importance of anelasticity in the interpretation of seismic tomography, *Geophys. Res. Lett.*, *20*(15), 1623–1626, doi:10.1029/93GL01767.

Karato, S., and B. B. Karki (2001), Origin of lateral variation of seismic wave velocities and density in the deep mantle, *J. Geophys. Res.*, *106*(B10), 21,771–21,783, doi:10.1029/2001JB000214.

Koelemeijer, P., J. Ritsema, A. Deuss, and H.-J. van Heijst (2016), SP12RTS: A degree-12 model of shear- and compressional-wave velocity for earth's mantle, *Geophys. J. Int.*, *204*(2), 1024–1039, doi:10.1093/gji/ggv481.

Masters, G., G. Laske, H. Bolton, and A. Dziewonski (2000), *The Relative Behavior of Shear Velocity, Bulk Sound Speed, and Compressional Velocity in the Mantle: Implications for Chemical and Thermal Structure*, chap. 3, pp. 63–87, AGU, Washington, D. C., doi:10.1029/GM117p0063.

McNamara, A. K., and S. Zhong (2005), Thermochemical structures beneath Africa and the Pacific Ocean, *Nature*, *437*, 1136–1139, doi:10.1038/nature04066.

Nakagawa, T., P. J. Tackley, F. Deschamps, and J. A. Connolly (2010), The influence of MORB and harzburgite composition on thermo-chemical mantle convection in a 3-D spherical shell with self-consistently calculated mineral physics, *Earth Planet. Sci. Lett.*, *269*(3-4), 403–412, doi:10.1016/j.epsl.2010.05.026.

Obayashi, M., J. Yoshimitsu, G. Nolet, Y. Fukao, H. Shiobara, H. Sugioka, H. Miyamachi, and Y. Gao (2013), Finite frequency whole mantle P wave tomography: Improvement of subducted slab images, *Geophys. Res. Lett.*, *40*, 5652–5657, doi:10.1002/2013GL057401.

Ritsema, J., A. K. McNamara, and A. L. Bull (2007), Tomographic filtering of geodynamic models: Implications for model interpretation and large-scale mantle structure, *J. Geophys. Res.*, *112*, B01303, doi:10.1029/2006JB004566.

Ritsema, J., H. J. van Heijst, J. H. Woodhouse, and A. Deuss (2009), Long-period body wave traveltimes through the crust: Implication for crustal corrections and seismic tomography, *Geophys. J. Int.*, *179*, 1255–1261, doi:10.1111/j.1365-246X.2009.04365.x.

Robertson, G. S., and J. H. Woodhouse (1996), Ratio of relative S to P velocity heterogeneity in the lower mantle, *J. Geophys. Res.*, *101*(B9), 20,041–20,052, doi:10.1029/96JB01905.

Romanowicz, B. A. (2001), Can we resolve 3D density heterogeneity in the lower mantle?, *Geophys. Res. Lett.*, *28*(6), 1107–1110, doi:10.1029/2000GL012278.

Saltzer, R. L., R. D. van der Hilst, and H. Kárason (2001), Comparing P and S wave heterogeneity in the mantle, *Geophys. Res. Lett.*, *28*(7), 1335–1338, doi:10.1029/2000GL012339.

Schuberth, B. S. A., H.-P. Bunge, and J. Ritsema (2009), Tomographic filtering of high-resolution mantle circulation models: Can seismic heterogeneity be explained by temperature alone?, *Geochem. Geophys. Geosyst.*, *10*, Q05W03, doi:10.1029/2009GC002401.

Simmons, N. A., A. M. Forte, L. Boschi, and S. P. Grand (2010), GyPSuM: A joint tomographic model of mantle density and seismic wave speeds, *J. Geophys. Res.*, *115*, B12310, doi:10.1029/2010JB007631.

Stixrude, L., and C. Lithgow-Bertelloni (2011), Thermodynamics of mantle minerals––II. Phase equilibria, *Geophys. J. Int.*, *184*(3), 1180–1213, doi:10.1111/j.1365-246X.2010.04890.x.

Su, W. J., and A. M. Dziewonski (1997), Simultaneous inversion for 3-D variations in shear and bulk velocity in the mantle, *Phys. Earth Planet. Inter.*, *100*(1-4), 135–156, doi:10.1016/S0031-9201(96)03236-0.

Tackley, P. J., S. Xie, T. Nakagawa, and J. W. Hernlund (2005), *Numerical and Laboratory Studies of Mantle Convection: Philosophy, Accomplishments, and Thermochemical Structure and Evolution*, chap. 6, pp. 83–99, AGU, Washington, D. C., doi:10.1029/160GM07.

Tesoniero, A., L. Auer, L. Boschi, and F. Cammarano (2015), Hydration of marginal basins and compositional variations within the continental lithospheric mantle inferred from a new global model of shear and compressional velocity, *J. Geophys. Res. Solid Earth*, *120*, 7789–7813, doi:10.1002/2015JB012026.

Trampert, J., F. Deschamps, J. Resovsky, and D. Yuen (2004), Probabilistic tomography maps chemical heterogeneities throughout the lower mantle, *Science*, *306*(5697), 853–856, doi:10.1126/science.1101996.

Wen, L., P. Silver, D. James, and R. Kuehnel (2001), Seismic evidence for a thermo-chemical boundary at the base of the Earth's mantle, *Earth Planet. Sci. Lett.*, *189*(3-4), 141–153, doi:10.1016/S0012-821X(01)00365-X.